Single-Stream Empirical Jet Noise Models Based on Scale-Model Data

Brenda S. Henderson[1]
National Aeronautics and Space Administration, John H. Glenn Research Center at Lewis Field, Cleveland, Ohio 44135, USA

Accurate single-stream jet-noise models for hot jets in flight are necessary for predicting noise of future commercial supersonic aircraft at takeoff. Previous comparisons between flight data and existing models have shown unacceptably large errors in the predictive tools. In the current effort, acoustic data were acquired in the Aero-Acoustic Propulsion Laboratory at the NASA Glenn Research Center for a single-stream hot jet with a range of operating conditions and simulated flight speeds that include those expected at takeoff of commercial supersonic aircraft. Models are presented for the resulting shape functions used to estimate the average spectra derived from the appropriate scaling of the jet-noise data.

I. Introduction

Renewed interest in commercial supersonic flight has led to an on-going noise-prediction effort for representative supersonic aircraft performing a range of take-off and landing procedures. Studies have shown jet noise to be a dominant source at lateral and flyover noise certification points and have highlighted the need for accurate predictions of jet noise [1]. Near-term entry-into-service aircraft are expected to be business jets with subsonic overland flight. Jet exhausts will likely be single streams resulting from mixed turbofan engines with speeds in the high subsonic to low supersonic range at takeoff. The dominant noise source for the jets is expected to be mixing noise. In an effort to quantify the error associated with current jet-noise prediction methods, a previous investigation compared scale-model jet noise data, existing jet noise prediction models, and flyover data acquired with a Learjet 25 [2]. The study was limited to prediction methods available in NASA's Aircraft Noise Prediction Program (ANOPP) [3]. The results of the study showed significant discrepancies between the predictions, flyover data, and scale-model data. The prediction methods used in the study included the SAE [4] and the Stone [5] models. The current investigation presents a dataset and new empirical prediction models for subsonic single-stream jets with flight. The models aim to improve predictions of jet noise at takeoff for future supersonic aircraft.

Jet-noise prediction generally falls into one of three approaches: empirical/semi-empirical models, acoustic analogies informed by Reynolds-averaged Navier-Stokes (RANS) solutions for the jet, and large-eddy simulations (LES) for the jet coupled with the Ffowcs-Williams Hawking approach [6] or its equivalent. For system-type studies where rapid predictions for noise are required, empirical/semi-empirical models are typically used. The models often use scaling based on jet-velocity or acoustic Mach number (ratio of the jet velocity to the ambient speed of sound) and can include models for the different noise sources in the jet. The present study is focused on models for system-type predictions.

Scaling of jet noise with jet velocity was first identified by Lassiter and Hubbard [7] whose early measurements indicated the overall-sound pressure varied with a power of the jet velocity with the power being slightly less than eight which supported Lighthill's velocity-to-the-eighth power scaling introduced slightly later [8]. This early jet study also noted the frequency of the peak amplitude increased with increasing jet velocity, a fact that supports the basis for Strouhal scaling typically used today. It is now recognized that the variation of jet noise with jet velocity depends on the emission angle with higher powers of the jet velocity being associated with radiation in the peak jet noise direction.

The use of SAE AIP876 (a precursor to SAE ARP876 Rev. F) for jet-noise predictions began in the early 1970s [9] at a time when flight data were limited. The SAE model predicts overall jet noise and one-third octave spectra for static jets (no flight) using jet velocity, temperature ratio, and nozzle diameter and then predicts jets in flight as a

[1] AIAA Associate Fellow

correction to the spectra for static jets. The approach uses Strouhal number and allows for a variation in the relative velocity exponent with emission angle. Recent comparisons with scale-model data [2] showed the SAE model outperformed other models used in the study although all models investigated did not adequately represent the measured data.

In addition to the SAE prediction standard, a number of jet-noise models and approaches are in use today. Tam et al. [10] developed two-source similarity spectra for the mixing noise of static jets, originally applied to supersonic jets, which account for sound generation from fine-scale and large-scale turbulence. While the models do not incorporate flight, a later investigation looked at the impact of flight on acoustic radiation [11]. The Stone [5] approach models noise sources in the jet, allows for flight, and has been extended to dual-stream jets. Recent comparisons with flight data [2] showed the Stone model outperformed the SAE model although neither approach adequately replicated the data. A review of jet-noise modeling may be found in [12].

A relatively recent approach which has included a significant investigation of the impact of multiple parameters on mixing noise may be found in [12, 13, 14, 15]. The most significant finding in this series of investigations was that jet noise spectra obtained at different jet pressures collapsed with the appropriate exponent of the acoustic Mach number when the nozzle temperature ratio (NTR), ratio of the jet stagnation temperature to the ambient temperature, was the same. Models for the resulting spectra were not presented although the velocity exponents obtained in the study were included and flight was addressed as a correction to the static jet as is done with the SAE standard. As in the case of SAE, the approach was focused on one-third octave spectra. In a recent study, this scaling approach was effectively applied to the SAE ARP876 models [16].

In the current investigation, single-stream empirical models are developed for constant NTRs as suggested in [12, 13, 14, and 15]. The models are for the prediction of narrowband data. The impact of flight is handled differently than in previous studies. The models are based on scale-model test data acquired in the Aero-Acoustic Propulsion Laboratory (AAPL) at the NASA Glenn Research Center. The prediction models and scale-model database will be compared to flight data in future reports.

II. Experiments

The experiments were performed in NASA's AAPL, a 65-ft radius geodesic dome treated with acoustic wedges (see Fig. 1). Within AAPL is the Nozzle Acoustic Test Rig (NATR) which produces a 53-in diameter simulated flight stream reaching Mach numbers of up to 0.35 and contains the High Flow Jet Exit Rig (HFJER), a three-stream jet-engine simulator capable of replicating most commercial turbofan-engine exhaust temperatures and pressures [17]. A single-stream conical nozzle with an exit diameter of 3.51-in was used in the experiments (see Fig. 2).

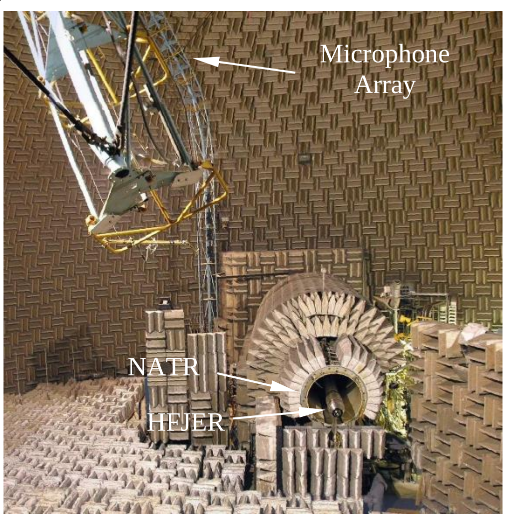

Figure 1. The Aero-Acoustic Propulsion Laboratory (AAPL) at the NASA Glenn Research Center.

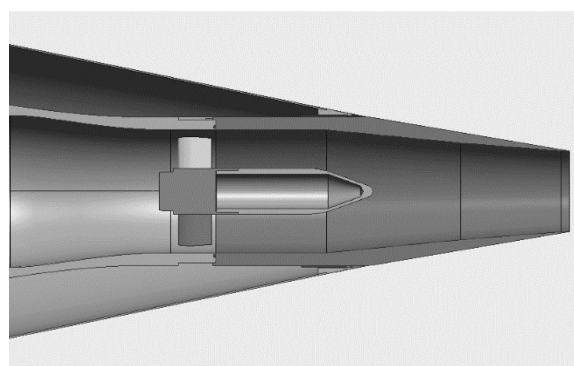

Figure 2. The conical nozzle used in the experiments.

Acoustic measurements were made with a 24-element far-field microphone array located on a 45-ft radius arc covering polar angles between 45° and 160° with angles greater than 90° in the downstream direction relative to the nozzle exit. Narrowband data with a 12.2-Hz binwidth were acquired for nozzle pressure ratios (NPRs) between 1.4 and 1.8, NTR between 1.5 and 3, and flight Mach numbers (M_{fj}) between 0.0 and 0.3. The NPR is given by the ratio of the jet stagnation pressure to the ambient pressure. Unless otherwise specified, data are presented as narrowband power spectral density, use emission coordinates, are not doppler shifted in frequency, are lossless, and are depropagated to a one-foot radial arc centered on the nozzle. The data are corrected for shear-layer refraction [18] assuming a source location at the nozzle exit. Microphone sensitivities and frequency responses were applied to the data.

III. Results

A. Comparisons with existing models (SAE ARP876)

A comparison between the data acquired at NPR = 1.8 and NTR = 2.5 and predictions from the SAE ARP876 model are shown in Fig. 3. The spectra are displayed in one-third octave as required for the SAE model and SPL is the sound pressure level. Near the broadside of the jet [see Figs. 3 (a) and (b)], the predicted and measured levels are close at the peak frequency. However, SAE underpredicts levels at high frequencies. Near the peak jet-noise angle [Fig. 3 (c)], SAE overpredicts the peak frequency and underpredicts the peak level. Previous comparisons have shown that the ability of the SAE model to accurately predict scale-model data is sensitive to jet conditions. A more detailed SAE comparison as well as comparisons with other jet models may be found in [2].

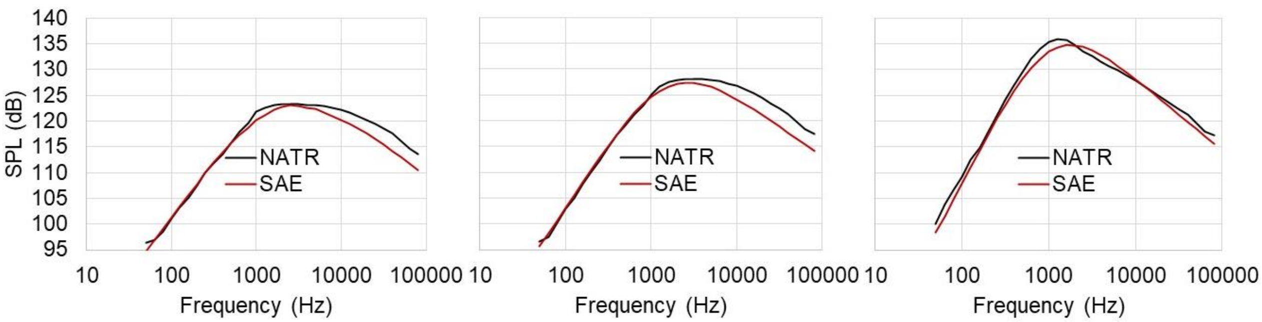

(a) (b) (c)

Fig. 3. A comparison between the data acquired at NPR = 1.8 and NTR = 2.5 and levels predicted by SAE ARP876 for emission angles equal to (a) 90°, (b) 110°, and (c) 130°.

B. Data Scaling

It has been shown previously [13] that a good collapse of jet-noise data is obtained when comparing results at the same NTR and emission angle if the spectra are properly scaled by a power of the acoustic Mach number and plotted as a function of Strouhal number (St), where $St = \frac{fD}{U}$, f is the frequency, D is the nozzle diameter, and U is the jet velocity. The resulting scaled spectra have nearly the same spectral shape. For the scaling and models presented here, the Mach number is given by the difference in the jet exhaust and simulated flight velocities divided by the ambient speed of sound. It should be noted that PSD is given by $10\log_{10}\frac{p^2}{p_{ref}^2 \Delta f}$, where p is the root-mean-square pressure at a particular discrete frequency, p_{ref} is the reference pressure of 20 μPa, and Δf is the binwidth in Hz.

The Mach-number scaling exponent is determined by minimizing the square error (E) defined as the difference in PSD amplitudes for a reference NPR and those acquired at other NPR over a range of St numbers of interest. The square error is given by

$$E = \sum_k \sum_l \{PSD_R(St_l) - 10n\log_{10} M_R - [PSD_k(St_l) - 10n\log_{10} M_k]\}^2 \qquad (1)$$

where M is the acoustic Mach number, the subscript R indicates measured quantities at the reference NPR, and the subscript k is used for quantities acquired at NPR other than the reference NPR. Minimizing E in the above equation with respect to n results in

$$n = \frac{\sum_k 10\log_{10}\left(^{M_R}/_{M_k}\right)\left[\sum_l PSD_R(St_l) - \sum_l PSD_k((St_l))\right]}{10l\sum_k\left[\log_{10}\left(^{M_R}/_{M_k}\right)\right]^2} \qquad (2)$$

for fixed NTR. The value of n depends on emission angle, M_{fj}, and is weakly dependent on NTR as will be shown later. In the current study, as the emission angle increased, the Strouhal numbers of interest in the above equation were decreased to a narrow range around the spectral peak as the data at high frequencies had a slight dependence on NPR in the aft emission quadrant so it was not possible to simultaneously match the spectral peaks and high frequency levels. Matching the peak levels was prioritized in the models presented here.

Once the value of n is determined, the Mach-number scaled data are averaged at each emission angle to obtain average Mach-numbered scaled data, where Mach number scaled PSD is given by

$$\text{Mach \# Scaled PSD} = PSD - 10n\log_{10} M, \tag{3}$$

and PSD is the measured power spectral density. The models in the next section are fit to the average Mach-number scaled data.

C. New Model

The proposed models fit a peak shape functions to the average Mach-number scaled power spectral density data. The models produce predictions for narrowband spectra. Note that scale factors are not applied to the data. Exponential functions [19, 20] are well suited to jet-noise data. In general, the sharper the peak the more complicated the function required to match the peak levels. The peaks of jet-noise spectra become sharper as the emission angle increases and the peak jet-noise angle is approached. The form of the function selected here balances ease of implementation with the ability to match peak levels.

The average Mach-number scaled power spectral density is modeled as a function of St and emission angle using the expression

$$PSD_M(St) = \frac{H}{\{1+\lambda_l \exp[(t_l - \log_{10} St)/k_l]\}^{m_l} + \{1+\lambda_t \exp[(\log_{10} St - t_t)/k_t]\}^{m_t} - 1}, \tag{4}$$

where the parameters $H, \lambda_l, \lambda_t, t_l, t_t, k_l, k_t, m_l$, and m_t, are determined by minimizing the difference in PSD_M and the average Mach-number scaled PSD data. In general, the parameters with subscripts l and t impact the leading and trailing edges of the shape functions, respectively, allowing for asymmetry with respect to the peak of the function. Jet-noise data requires a function that can fit asymmetric spectral shapes. The parameters t_l and t_t determine the location (with respect to St) of the leading and trailing edges of the function which impacts the location of the peak Strouhal number. The parameter H effects the peak level. The parameters m_l, and m_t impact the roll-off of PSD_M with St for the leading and trailing edges of the function. The remaining parameters (λ_l, λ_t, k_l, and k_t) impact the general shape of the function. It will be shown later that some of the parameters are functions of only the emission angle while others are functions of the emission angle, NTR, and M_{fj}.

The models are developed for the static jet first then slightly modified to fit the data acquired with a flight stream. For the flight-stream conditions, it was found that reasonable agreement between the model and data was obtained for all emission angles except 140° by modifying the values of λ_t and H from those used for the static jet. For an emission angle of 140°, it was also necessary to modify the value of m_l for some NTR and M_{fj}. The values for the model parameters will be discussed in subsequent sections.

D. Scaled Data and Models for Static Jets

The scaled data acquired at NTR = 2.5 and their corresponding averages are shown in Fig. 4. A good collapse of the spectra is found for all emission angles. Similar results were obtained at other NTR except near the peak jet-noise angle for the highest temperature and pressure ratios used in the study (NPR = 1.8, NTR = 3.0) where the collapse of the data was not as good.

The values of the Mach-number exponent, n, are provided in Fig. 5. The data in Fig. 5 (a) show the variation of n with NTR and emission angle. The velocity exponent increases with increasing emission angle except for the lowest NTR (1.5) and the smallest emission angles (80° and 90°). There is also some dependency of n on NTR most notably at the smaller emission angles in Fig. 5 (a). The data for all NTR are shown in Fig. 5 (b) except for NTR = 1.5 and emission angles of 80°and 90° along with a best fit curve.

The shape functions obtained using Eq. 4 and the averaged data are shown in Fig. 6 for NTR = 2.5. Reasonable agreement is obtained between the models and data at all emission angles. The selected shape function captures the sharp peaks at 140°. Similar results were obtained at other NTR and emission angles except for NTR = 3.0 at 140° where the Mach-number exponent data collapse was not adequate.

The shape function parameters for Eq. (4) as a function of emission angle are shown in Figs. 7 and 8. The values for the parameters in Fig. 7 are independent of NTR. The parameters in Fig. 8 depend on NTR and emission angle. Also included in Fig. 8 are best fit curves for the data. The color scheme used for the curve-fit equations is the same as that used in the legend for NTR.

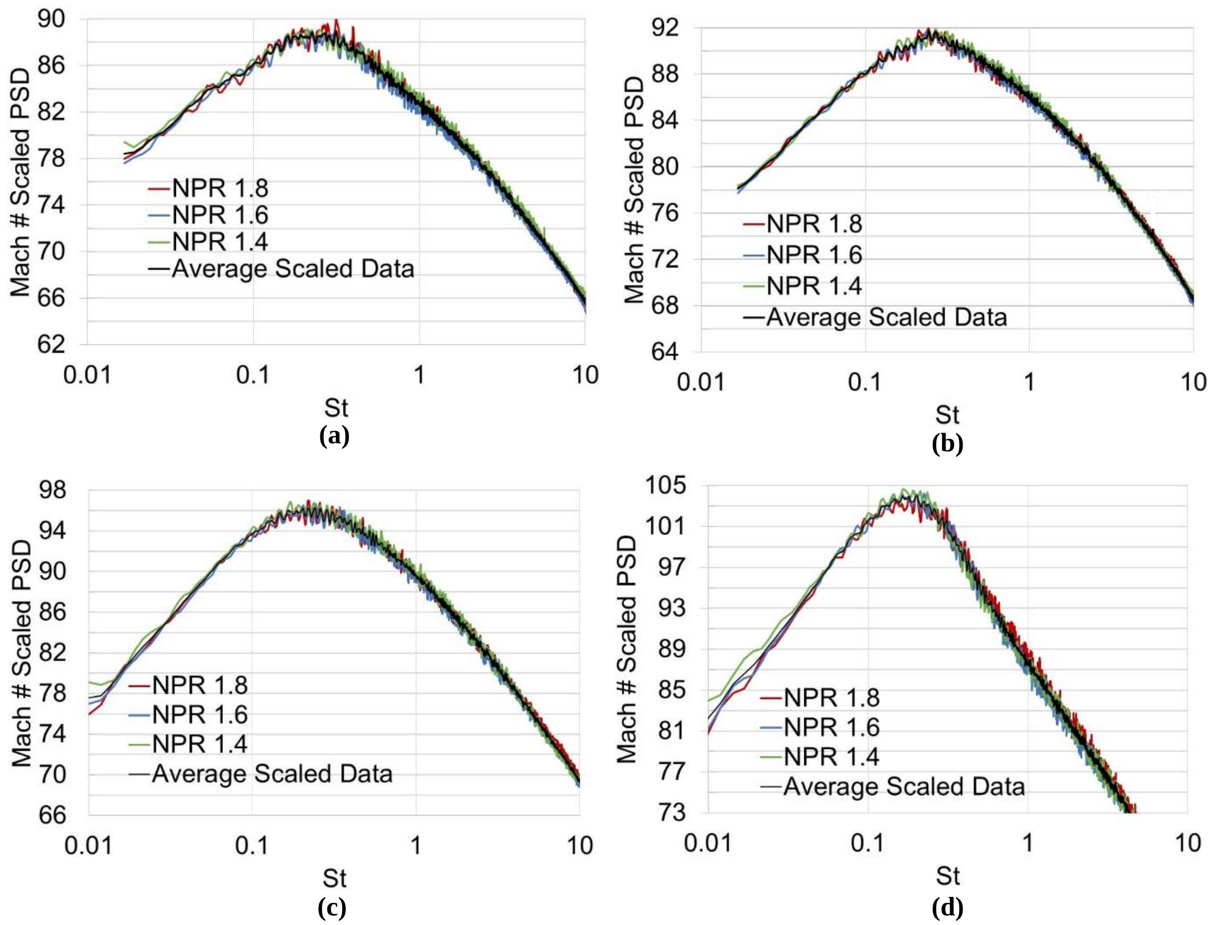

Figure 4. The scaled and their averages for the static jet at NTR = 2.5 and emission angles of (a) 80°, (b) 100°, (c) 120°, and (d) 140°.

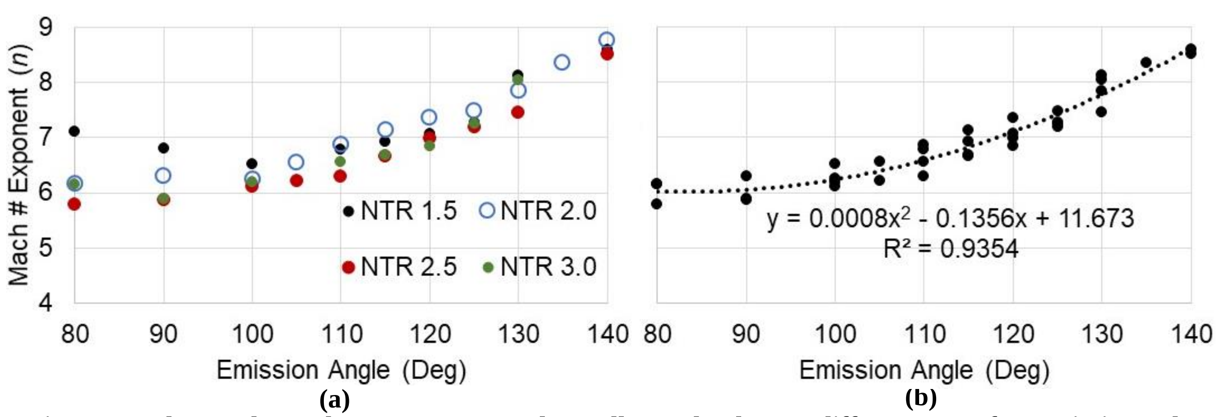

Figure 5. The Mach number exponents used to collapse the data at different NPR for static jets. The data in (a) show the variation in the exponent with angle and NTR. The data in (b) include all NTR except for NTR = 1.5 at 80° and 90°. Also shown in (b) is a best fit curve through the included data.

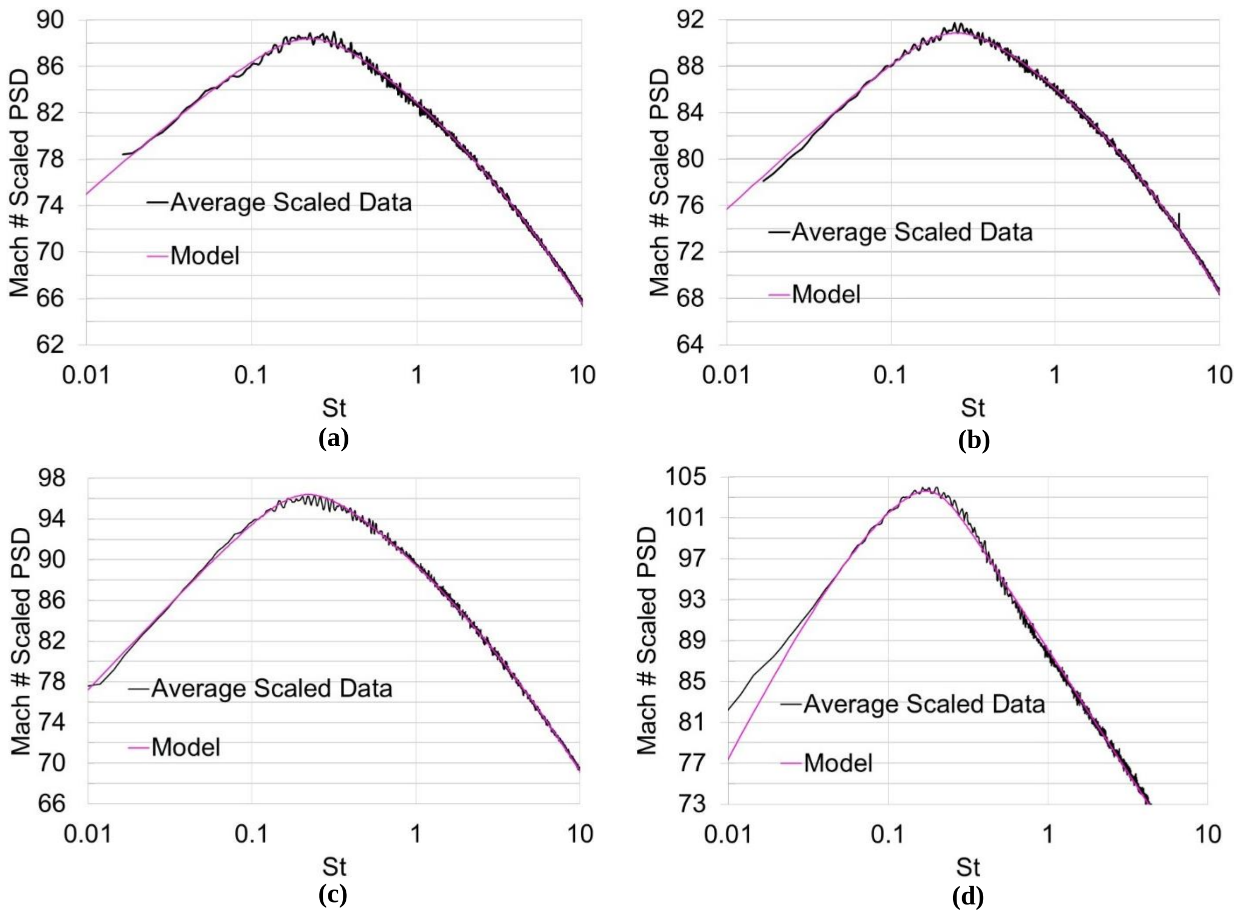

Figure 6. The averaged data and modeled spectra for the static jet at NTR = 2.5 and emission angles of (a) 80°, (b) 100°, (c) 120°, and (d) 140°.

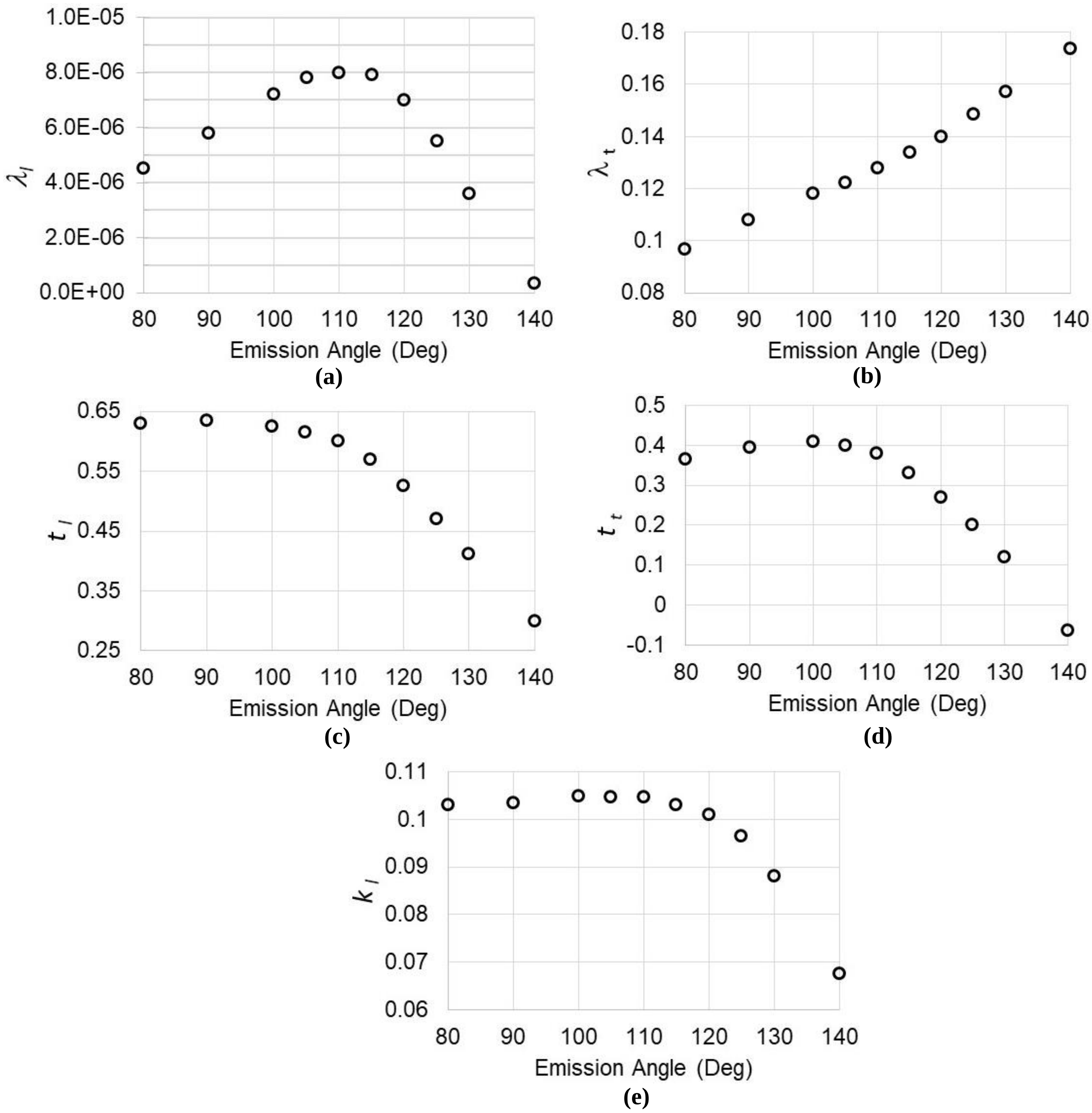

Fig. 7. The shape function parameters used in Eq. (4) for (a) λ_l, (b) λ_t, (c) t_l, (d) t_t, and (e) k_l for static jets.

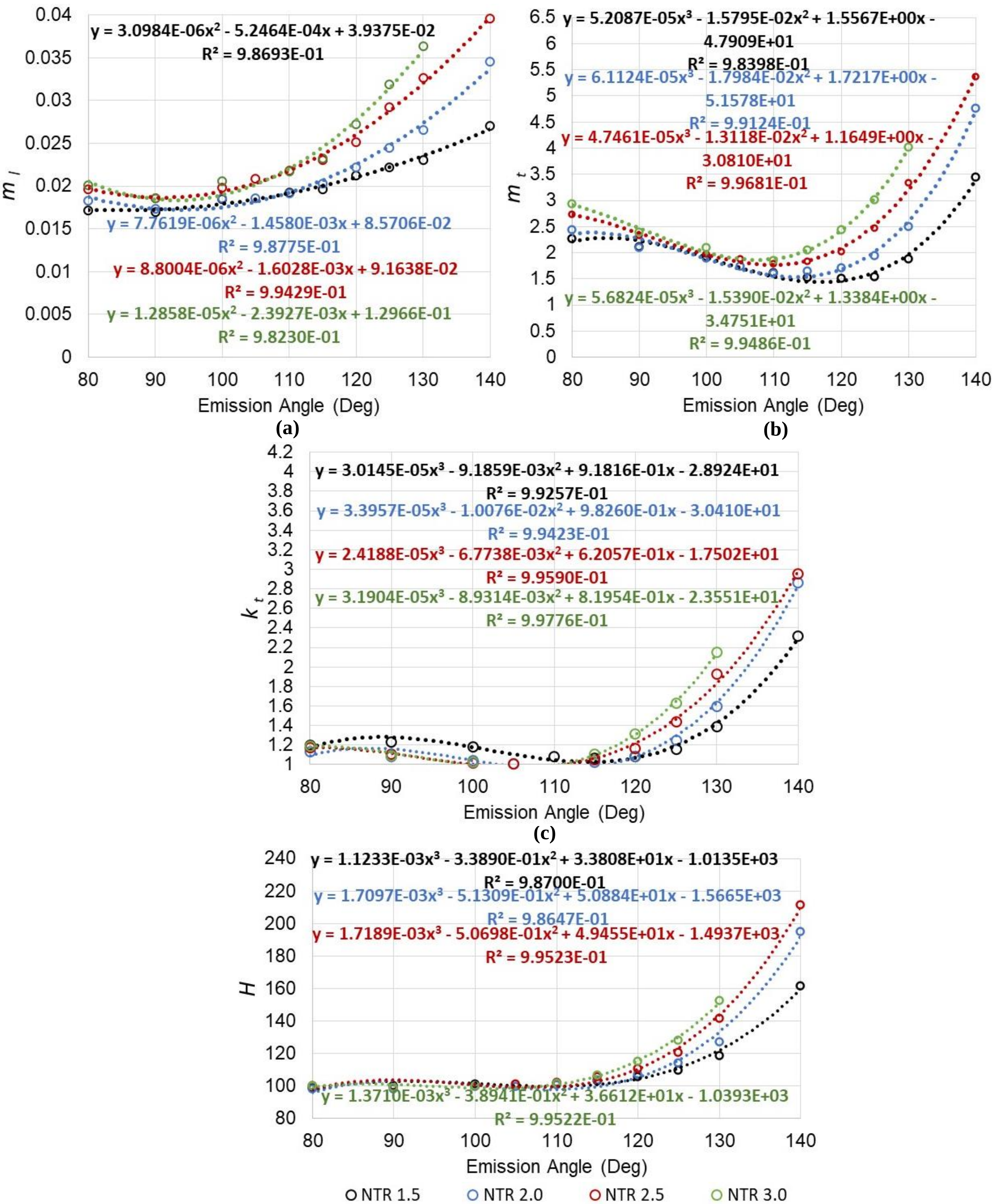

(d)

Fig. 8. The shape function parameters and corresponding best fit curves (dashed curves and equations) for (a) m_l, (b) m_t, (c) k_t, and (d) H at static jets.

E. Scaled Data and Models for Jets with Flight Streams

The spectra obtained at an NPR = 1.8, NTR = 2.5, and M_{fj} equal to 0.0 and 0.3 are shown in Fig. 9. The levels for the static jets are higher than those for M_{fj} = 0.3 as expected, with the reductions associated with the flight stream being greater in the peak jet-noise direction than near the broadside of the jet. Additionally, the introduction of the flight stream impacts the peak levels more than the high-frequency levels. The effect of the flight stream on peak levels in the peak jet-noise direction is likely due to the impact of flight on large-scale structures in the jet.

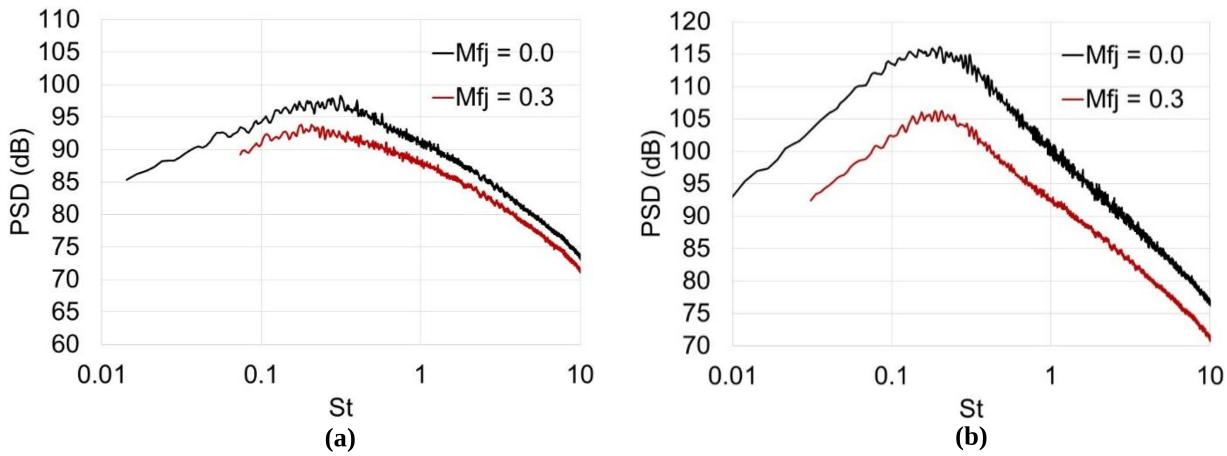

Fig. 9. The PSD acquired at NPR = 1.8, NTR = 2.5 and (a) 80° and (b) 140°.

Comparisons of the Mach-number scaled and averaged data are shown in Fig. 10 for NTR = 2.5 and M_{fj} = 0.2. Note the Mach-number scaling uses a velocity given by the difference in the jet exit velocity and the flight-stream velocity. A reasonable collapse of the data is found for all emission angles although there is a slight offset between the different NPR datasets at high frequencies for an observation angle of 140° which is difficult to see in the Figure. The high frequency offset is slightly more pronounced in the data for M_{fj} = 0.3 than at lower flight Mach numbers.

The Mach number exponents, *n*, as a function of emission angle are shown in Fig. 11 for different flight Mach numbers. The exponent is a function of emission angle and M_{fj}. The exponent is also a weak function of NTR.

Comparisons between the average scaled data obtained at NTR = 2.5 and flight Mach numbers between 0.0 and 0.3 are shown in Fig. 12. As the flight Mach number increases, the high frequency levels increase relative to the peak levels for emission angles greater than, or equal to, 100°. The increases in levels at high-frequency are greater in the peak jet-noise direction than at angles near the broadside of the jet. Similar trends were observed at other NTR.

The averaged data and spectra obtained from the models for NTR = 2.5 and M_{fj} equal to 0.0 and 0.3 are shown in Fig. 13. For all emission angles except for 140°, only λ_t and *H* were changed from those for M_{fj} = 0.0 to fit the M_{fj} = 0.3 data. For 140°, it was necessary to change m_l, λ_t, and *H* to fit the M_{fj} = 0.3 data. The aim was to change as few parameters as possible between the static jet and flight conditions to simplify implementation of the models. Similar trends to those shown in Fig. 13 were obtained at other NTR and flight Mach numbers. The greatest discrepancies between the models and average spectra were typically associated with the highest M_{fj} (0.3), and the largest emission angle (140°).

Table 1 Values of m_l at 140°

	Mfj		
	0.1	**0.2**	**0.3**
NTR = 1.5	No Change	No Change	No Change
NTR = 2.0	No Change	No Change	0.0335
NTR = 2.5	0.0385	0.0349	0.035
NTR = 3.0	0.0475	0.043	0.0425

Plots of λ_t and *H* as a function of emission angle are shown in Figs. 14 and 15, respectively. The values for m_l are shown in Table 1 where "No Change" indicates the values are the same as those for the static jet. For all flight conditions, both λ_t and *H* increase with increasing angle for angles greater than 110°.

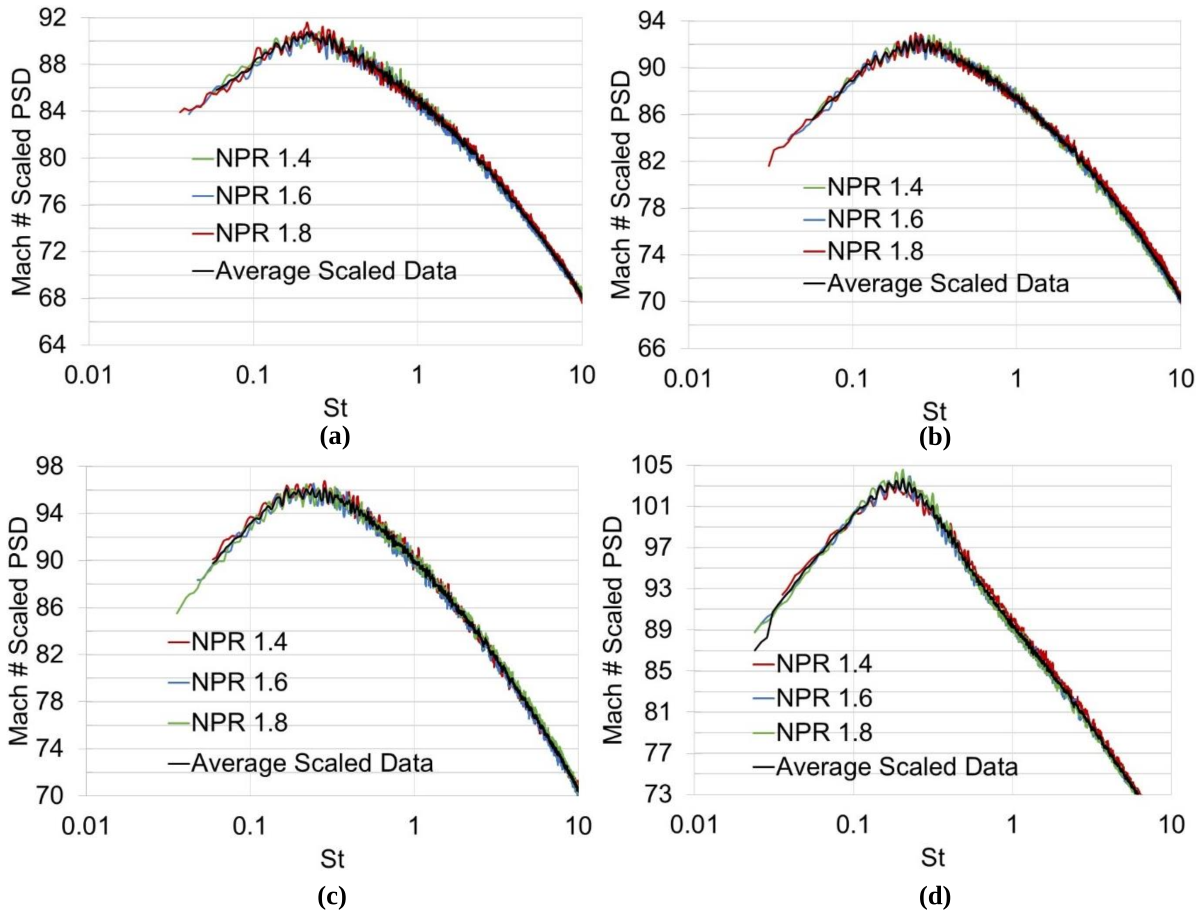

Fig. 10. The scaled data and their averages for NTR = 2.5 and a flight Mach number of 0.2 at emission angles equal to (a) 80°, (b) 100°, (c) 120°, (d) 140°.

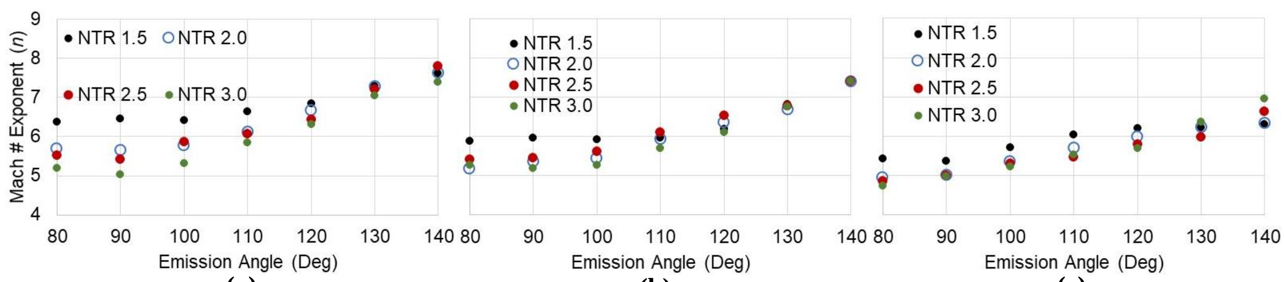

Fig. 11. The Mach number exponents at the indicated NTR for (a) M_{fj} = 0.1, (b) M_{fj} = 0.2, and (c) M_{fj} = 0.3.

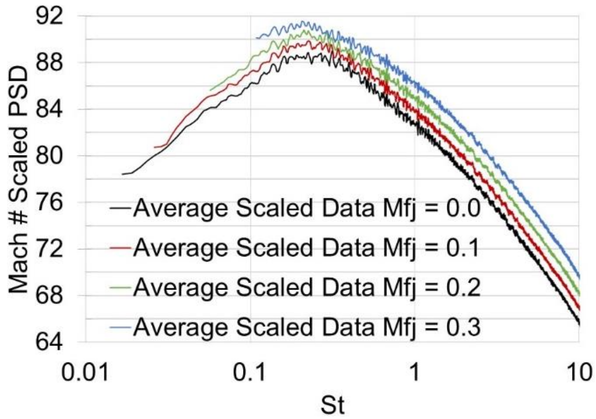

(a)

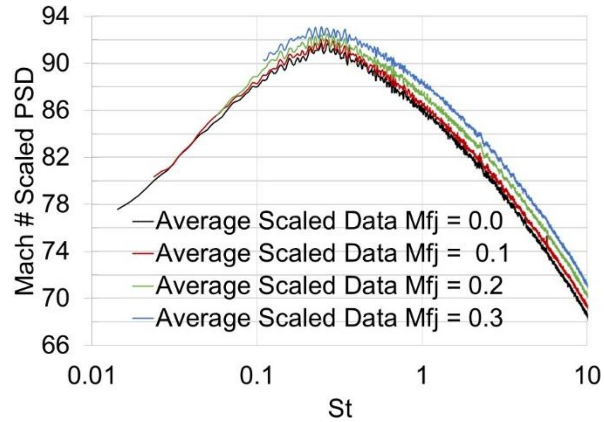

(b)

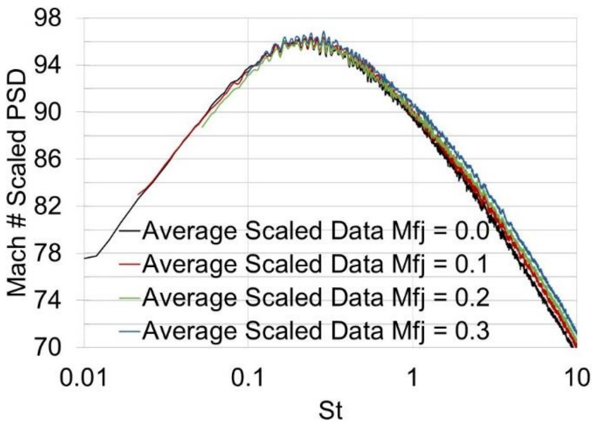

(c)

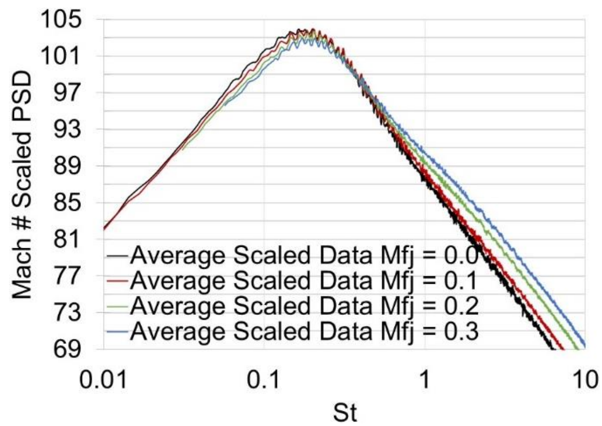

(d)

Fig. 12. The averaged data for NTR = 2.5 and the indicated flight Mach numbers. The emission angles are (a) 80°, (b) 100°, (c) 120°, and (c) 140°.

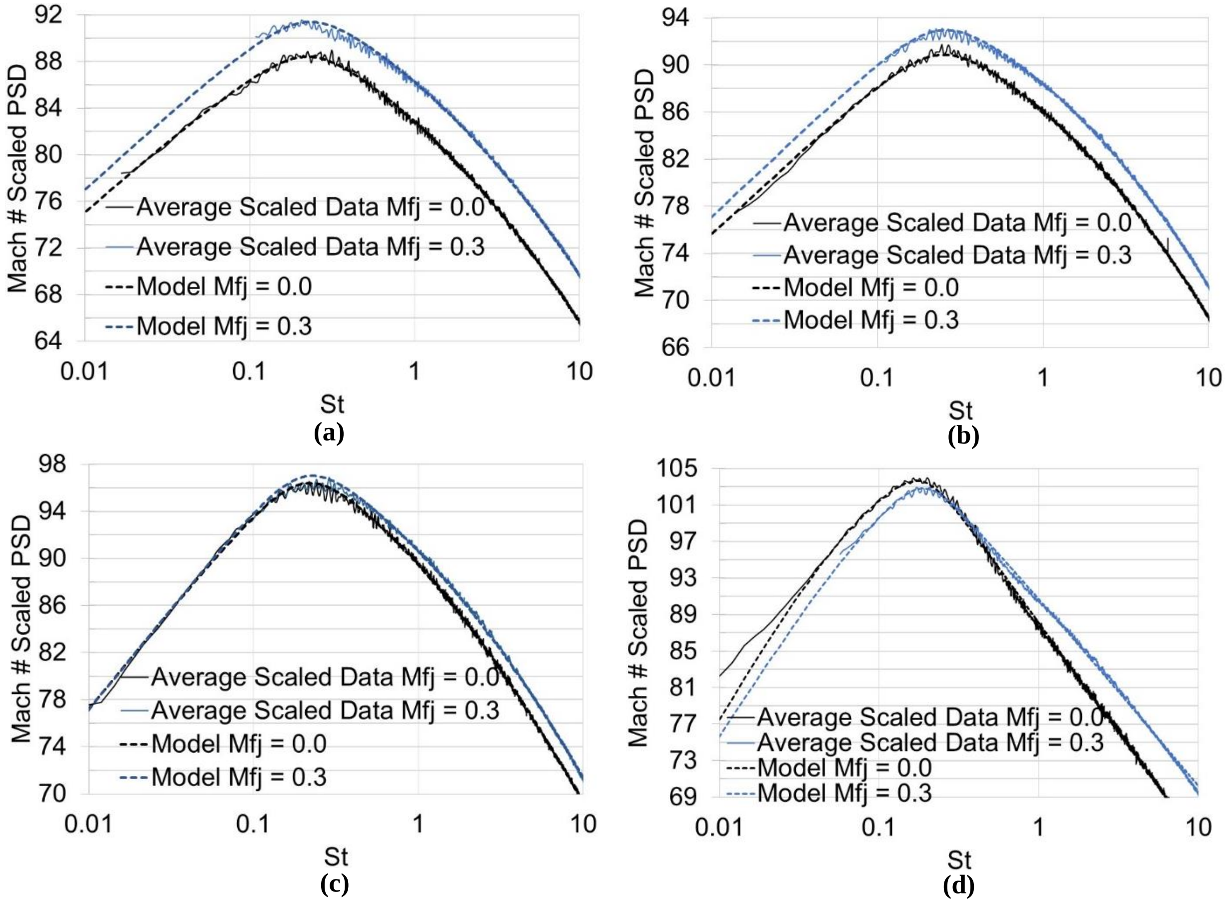

Fig. 13. The average spectra and modeled spectra for NTR = 2.5 and flight Mach numbers equal to 0.0 and 0.3. The emission angles are (a) 80°, (b) 100°, (c) 120°, and (c) 140°.

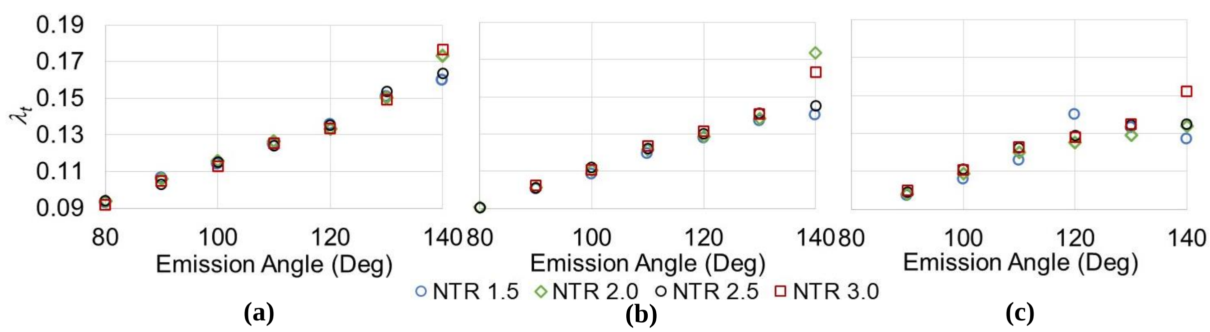

Fig. 14. The values of λ_t as a function of emission angle for M_{fj} equal to (a) 0.1, (b) 0.2, and (c) 0.3.

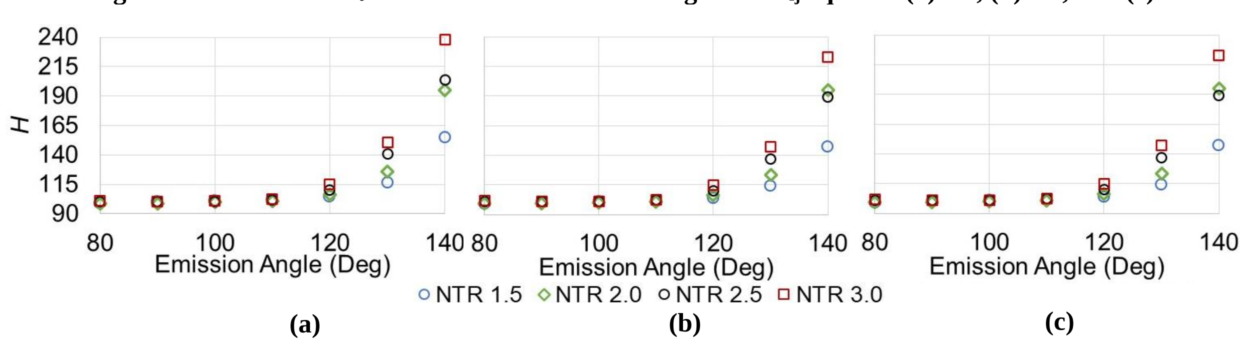

Fig. 15. The values H as a function of emission angle for M_{fj} equal to (a) 0.1, (b) 0.2, and (c) 0.3.

IV. Conclusions

A dataset intended for the development of single-stream jet noise models was acquired for the purpose of improving jet-noise predictions for supersonic aircraft at takeoff. The engine exhausts of these aircraft are expected to be at high subsonic to low supersonic speeds at takeoff and the acoustic radiation is expected to be dominated by mixing noise. Models were developed from the dataset for the prediction of static and flight conditions with nozzle pressure ratios between 1.4 and 1.8, nozzle temperature ratios between 1.5 and 3.0, and flight Mach numbers between 0.0 and 0.3. For emission angles between 80° and 140°, agreement between models and the data is quite good for most jet and flight conditions covered by the test campaign. A single nozzle was used for the dataset and, therefore, the data and models have been presented for the diameter used in the experiments.

References

[1] Berton, J. J., Jones. S., Seidel, J. and Huff, D., "Noise Predictions for a Supersonic Business Jet Using Advanced Take-Off Procedures," *Aeronaut. J.*, Vol. 122, No. 1250, 2018, pp. 556 – 571.

[2] Henderson, B. S.., Huff, D. L. Berton, J. J., "Jet Noise Prediction Comparisons with Scale Model Tests and Learjet Flyover Data," AIAA Paper 2019-2768, 2019, June 2019.

[3] Zorumski, W. E., "Aircraft Noise Prediction Program Theoretical Manual, Parts 1 and 2," NASA TM-83199, 1982.

[4] *Gas Turbine Jet Exhaust Noise Prediction*., SAE Aerospace Recommended Practice ARP876, Society of Automotive Engineers, March 1978.

[5] Stone, J. R., Krejsa, E. A, Clark, B. K. and Berton, J. J., "Jet Noise Modeling for Suppressed and Unsuppressed Aircraft in Simulated Flight," NASA TM-2009-215524, 2009.

[6] Ffowcs Williams, J. E., Hawkings, D. L., "Sound Generation by Turbulence and Surfaces in Arbitrary Motion," *Philos. Trans. R. Soc. London Ser A Math Thys, Sci*,, Vol. 264, No. 1151, 1969, pp. 321 – 342.

[7] Lassiter, L. W. and Hubbard, H., "Experimental Studies of Noise from Subsonic Jets in Still Air," NACA-TN-2757, 1952.

[8] Lighthill, M. J., "On Sound Generated Aerodynamically. I. General Theory," *Proc. R. Soc. Lond. A*., Vol. 211, 1952, pp. 564-587.

[9] General Electric Company, "Propulsion System Studies for an Advanced High Subsonic Long Range Jet Commercial Transport Aircraft," NASA-CR-121016, 1972.

[10] Tam, C. K. W., Golebiowski, M., and Seiner, J., "On the Two Components of Turbulent Mixing Noise from Supersonic Jets," AIAA Paper 1996-1716, 1996.

[11] Tam. C. K. W., Pastouchenko, N., and Auriault, L., "The Effects of Forward Flight on Jet Mixing Noise from Fine Scale Turbulence," AIAA Paper 2000-2061, 2000.

[12] Viswanathan, K, "Scaling Laws and a Method of Identifying Components of Jet Noise," *AIAA J*., Vol. 44, No. 10, 2006, pp. 2274 – 2285.

[13] Viswanathan, K. and Czech, M. J., "Improved Method for Prediction of Noise from Single Jets," *AIAA J.*, Vol. 45. No. 1, 2007, pp. 151-161,

[14] Viswanathan, K. and Czech, M. J., "Role of Jet Temperature in Correlating Jet Noise," *AIAA Journal*, Vol. 47, No. 5, 2009, pp. 1090-1106.

[15] Viswanathan, K. and Czech, M. J., "Measurement and Modeling of Effect of Forward Flight on Jet Noise," *AIAA J.*, Vol. 49, No. 1, 2011, pp. 216-234.

[16] Akatsuka, J. and Ishii, T., "Comparative Study of Semi-Empirical Jet Noise Prediction Models for Future Commercial Supersonic Aircraft," AIAA Paper 2021-2219, June 2021.

[17] Soeder, R. H., Wnuk, S. P., and Loew, R, "Aero-Acoustic Propulsion Laboratory Nozzle Acoustic Test Rig User Manual," NASA TM-2006-212939, 2006.

[18] Ahuja, K. K., and Tester, B. J., "The Free Jet as Simulator of Forward Velocity Effects on Jet Noise," NASA CR 3056, 1978.

[19] Li, J, "Development and Evaluation of Flexible Empirical Peak Function for Processing Chromatographic Peaks," *Anal. of Chem.*, Vol. 69, 1997, pp. 4452-4462.

[20] Li., J, "Comparison of Capability of Peak Functions in Describing Real Chromotographic Peaks," *J. Chromotography A*, Vol. 952, 2002, pp. 63-70.